IEEE Access
Multidisciplinary | Rapid Review | Open Access Journal

Received March 5, 2020, accepted March 19, 2020, date of publication March 23, 2020, date of current version April 1, 2020.

*Digital Object Identifier 10.1109/ACCESS.2020.2982462*

# Analysis of Nonlinear Dynamics of Permanent Magnet Magnetic Contactor via Novel Computationally Efficient Analytical Method Considering Stray and Leakage Fluxes

**NIKITA GABDULLIN, (Member, IEEE), AND JONG-SUK RO, (Member, IEEE)**
School of Electrical and Electronic Engineering, Chung-Ang University, Seoul 06974, South Korea

Corresponding author: Jong-Suk Ro (jongsukro@gmail.com)

This work was supported in part by the Basic Science Research Program of the National Research Foundation of Korea funded by the Ministry of Education under Grant 2016R1D1A1B01008058, and in part by the Human Resources Development of the Korea Institute of Energy Technology Evaluation and Planning (KETEP) Grant funded by the Korea Government Ministry of Trade, Industry and Energy under Grant 20204030200090.

**ABSTRACT** Improving the efficiency and end-use of energy distribution can significantly reduce global energy consumption. As the magnetic contactor (MC) is the most common switchgear used for control in most grids, minimizing its energy consumption has motivated the development of a permanent magnet (PM) MC that exhibits several advantages over conventional solenoid MCs. However, analyzing the transient magnetic behavior of a PM MC requires computationally expensive 3D finite element analysis (FEA). Herein, a modified version of a recently proposed nonlinear transient path energy method (NT-PEM) is proposed as an analytical alternative to FEA. Within the modification to NT-PEM, a new topology for nonlinear dynamic magnetic equivalent circuit (ND-MEC) is proposed with a methodology for accurate evaluation of stray and leakage flux path parameters. For coil leakage reluctances, a novel path function based on a conchoid's arc is proposed. For stray reluctances, a path function based on the average length of an elliptical arc is proposed. This path function, along with the proposed permeability correction for nonlinear core reluctance calculation routines, led to a four-fold reduction in NT-PEM analysis time from the original version of the proposed method. The feasibility of the proposed NT-PEM is verified via comparison with commercial 3D FEA and experimental data obtained from a PM MC with a single coil and single PM. NT-PEM and FEA equally displayed accurate results, indicating that NT-PEM is a promising computationally efficient alternative to FEA owing to significantly reduced analysis time, which is essential when considering numerous designs and design parameters.

**INDEX TERMS** Magnetic contactor, MEC, nonlinear dynamics, NT-PEM, permanent magnets, stray flux modeling.

## I. INTRODUCTION

In recent decades, the efficiency of electrical energy generation, distribution, and consumption have been topics of growing significance owing to the concerns regarding the future impending depletion of currently available energy resources and the environmental impact of conventionally acceptable yet damaging energy generation and consumption practices. This topic is particularly important for the industrial sector, which, for instance, in the US contributes to more than 30% of the total energy consumption and up to 40% of the $CO_2$ emissions [1], [2].

Therefore, devices that connect consumers in electrical grids, such as relays and magnetic contactors (MCs), show remarkable potential to reduce energy consumption significantly. This has led to the development of permanent magnet (PM) MCs that consume less or even no energy in a closed state, unlike conventional solenoid MCs. The widespread of

The associate editor coordinating the review of this manuscript and approving it for publication was Yan-Jun Liu.

PM MCs can be illustrated by their relevance for industrial applications, consumers, and recent AC and DC renewable energy grids [3]–[5].

To address the drawbacks of conventional solenoid MCs, Fang *et al.* [6] and Shu *et al.* [7] developed PM MCs that significantly reduce energy consumption and utilize smart control to improve dynamic characteristics. Wang *et al.* have shown the feasibility of PM MCs for voltages as high as 126 kV [8]. Park *et al.* [9] proposed a PM MC that required a relatively large current of 10 A and active electronics for its control. To improve the reliability of PM MCs and reduce the required current, Bak *et al.* [10] proposed an electronically controlled PM MC with two coils, with the main PM positioned on the armature and an additional PM as part of an interlocking mechanism. However, it should be noted that requiring control circuitry substantially increases price of the PM MC making electronics-free PM MC desirable [11]–[13].

This study investigates the feasibility of PM MCs with a single coil and single PM, with a capacitor charged during closing used for PM MC opening. However, the focus is on the accuracy and computational efficiency of the analysis method used to evaluate the dynamics of the PM MC. PM MC analysis is significantly more complicated than solenoid MC's owing to the mutual interaction between the PM and coil magnetic fields. Computationally expensive 3D finite element analysis (FEA) is commonly employed for electromagnetic analysis and design [14]. PM MC FEA leads to extremely long analysis times, especially when numerous designs must be considered. This motivates the proposal of an efficient analytical method as an alternative to FEA [15], [16], with a magnetic equivalent circuit (MEC) method commonly used for electrical machine design and analysis [17].

However, PM MCs are characterized by complex magnetic field distribution that changes depending on the operating regime of the MC, which cannot be accurately represented in conventional MECs. First, this drawback is due to the significant stray and leakage fluxes characterized by flux paths of complex geometry [18]. These paths are conventionally oversimplified in MEC models, thus decreasing the accuracy of the analysis. Second, the motion of MC armature alters the parameters of MEC, hence requiring the MEC to account not only for a more studied core nonlinearity, but for nonlinearities and spatial dynamic changes in the magnetic circuit [19].

To address these problems and propose an accurate and computationally inexpensive analysis method, this study builds on a recently proposed nonlinear transient path energy method (NT-PEM) that exploits a nonlinear dynamic magnetic equivalent circuit (ND-MEC) to account for both stray path reluctances and dynamic nonlinearities. However, this method is modified in this study to further improve the analysis speed by reducing the number of iterative routines. Both the attraction and repulsion modes are considered, and the ND-MEC topology that accounts for flux paths in both regimes is also proposed. Furthermore, a new mathematical representation of coil leakage reluctances using a conchoid function is proposed.

Further Sections of this paper are organized as follows: Section II proposes a single ND-MEC and describes conventional core and main air path reluctances; Section III discusses more complex stray path and leakage reluctances and proposes elliptical and conchoid functions for their modeling; Section IV outlines the method for solving the ND-MEC equations for flux calculation; Section V discusses the electromagnetic force calculation by extending ND-MEC to time domain via the proposed modified NT-PEM along with the electrical circuit and armature motion equations; Section VI summarizes the results of the analysis providing the experimental verification and discusses the advantages of the modified NT-PEM over original NT-PEM and FEA; Section VII provides the conclusions and closing remarks.

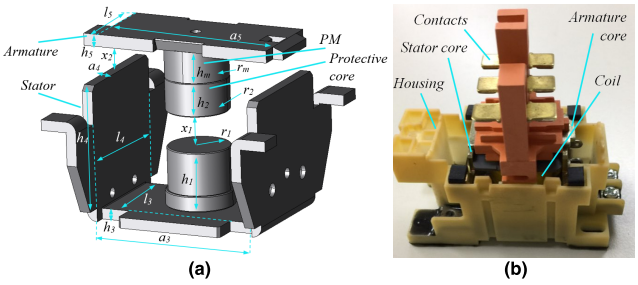


**FIGURE 1.** (a) Magnetic circuit and design parameters of the investigated PM MC with a single coil on the stator (not shown) and single PM on armature; (b) prototype of the single-coil PM MC.

## II. FORMULATION OF ND-MEC AND MAIN FLUX PATH RELUCTANCES

### A. FORMULATION OF ND-MEC FOR PM MCS

As mentioned earlier, there are two main challenges that the PM MC shown in Fig. 1 poses to MEC analysis. First, a significant portion of the total magnetic flux generated by the PM and coil is attributed to stray magnetic fluxes that flow outside the main flux paths. Second, closing and opening regimes utilize both magnetic attraction and repulsion, leading to significant variations in magnetic field distribution in these two regimes. Hence, the MEC of the PM MC must account for both stray air paths and allow flux redistribution to be taken into account accurately.

This study proposes an ND-MEC shown in Fig. 2 that considers both core magnetic non-linearities and the variation of stray path reluctances with armature displacements. The main advantage of the proposed ND-MEC is its ability to model both PM MC regimes, as shown in Fig. 3. Fig. 3 (a) shows that during closing operation, the linked flux primarily follows the main flux path with $R_{13s}$, $R_{14s}$, and $R_{ms}$ in Fig. 2 (a) acting as leakage reluctances. In contrast, these stray paths allow for the fluxes during repulsion to be modeled, as shown in Fig. 3 (b). The contributions of different flux paths to the electromagnetic force can also be conveniently adjusted depending on attraction/repulsion, as discussed in Section V.

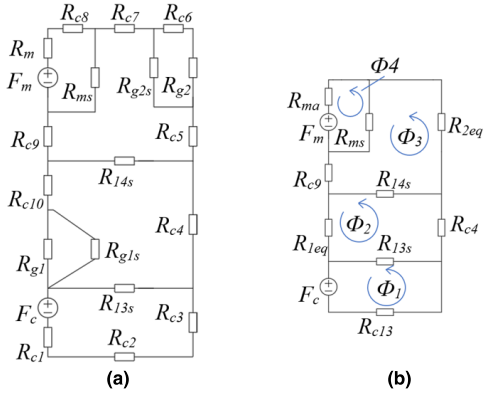


**FIGURE 2.** Proposed ND-MEC topology for the studied PM MC that accounts for both the closing and opening regimes; (a) the complete ND-MEC that includes all stray and leakage reluctances for accurate flux distribution representation, (b) reduced ND-MEC for flux calculation.

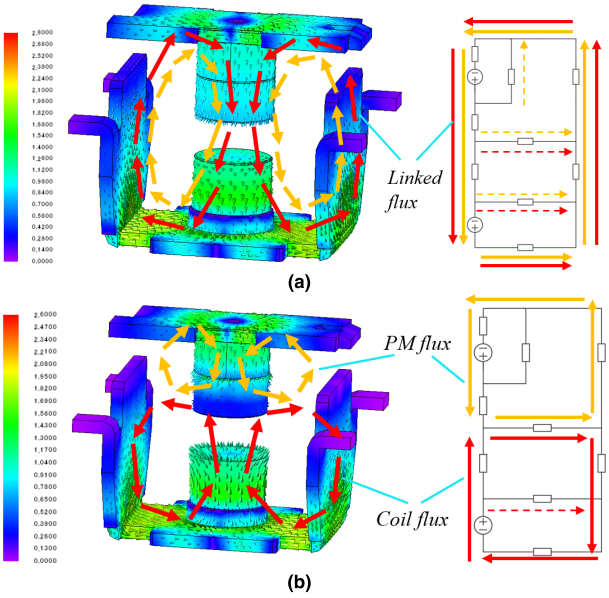


**FIGURE 3.** Magnetic flux density distribution and flux density vector field in the magnetic circuit of PM MC and the corresponding orientation of fluxes in the branches of the proposed ND-MEC for (a) electromagnetic attraction during closing and (b) electromagnetic repulsion during opening operation. Dashed lines represent leakage fluxes. Colors represent the magnitude of flux density *B* in T.

### B. FORMULATION OF NONLINEAR CORE RELUCTANCES

#### 1) GENERALIZED EXPRESSION FOR CORE RELUCTANCES

Modeling core reluctance $R_c$ is an extensively investigated topic [20], [21], which allows a general expression for each of $i = 1..10$ core regions in Fig. 2 to be expressed as:

$$R_{ci} = \frac{k_{ci} l_{ci}}{\mu_{ri} \mu_0 A_{ci}}, \tag{1}$$

where $k_c$ accounts for the symmetry in the circuit

$$k_{ci} = \begin{cases} 0.5, & i = 2-9; \\ 1, & i = 1, 10, 11. \end{cases} \tag{2}$$

Similarly, the PM reluctance $R_m$ is calculated as:

$$R_m = \frac{h_m}{1.05\pi \mu_0 r_m^2}. \tag{3}$$

Finally, sources in Fig. 2 correspond to magnetomotive forces (mmf) due to coil and PM that are calculated as:

$$F_c = I_c w_c \tag{4}$$

$$F_m = h_m H_c, \tag{5}$$

where $I_c$ is the coil current in A, $w_c$ is the number of coil turns, and $H_c$ is the coercive force of PM in A/m.

#### 2) ACCOUNTING FOR NONLINEAR MAGNETIC PROPERTIES

Because nonlinearities associated with core reluctances are typical for all MECs, representing a nonlinear *B-H* curve of the steel with a $\mu_c(H)$ function is a common approach comprehensively addressed in previous studies [17], [22]. However, the computational efficiency and accuracy of the approximation must be considered. This study uses a recently proposed rational approximation [23], which allows the absolute core permeability of an $i^{th}$ core reluctance to be represented as shown below:

$$\mu_{ci}(H_i) = \frac{168}{H_i + 7.4 \cdot 10^6} + \frac{1.55}{H_i + 239} + \frac{0.09 \cdot (H_i - 27)}{(H_i - 34)^2 + 42^2}. \tag{6}$$

The ND-MEC, as well as other nonlinear MEC methods, requires (6) to be evaluated iteratively, minimizing error in flux density [24]. However, it was found that the original permeability correction significantly increases computational costs, particularly when high accuracy is required. To ensure fast convergence while minimizing numerical errors, a modified core permeability expression is proposed:

$$\mu_{ci}^n = \frac{\mu_{ci}(H_i)^2 + b(\mu_{ci}^{n-1})^2}{(b+1)\mu_{ci}^{n-1}}, \begin{cases} b = 4, & B_i < 1 \\ b = 1, & B_i \geq 1 \end{cases} \tag{7}$$

where $B_i$ is the magnetic flux density in T before permeability correction. Equation (6) allows for rapid converging and is robust against numerical errors. This characteristic is due to the *n-1* step information being used as a weight, preventing abrupt changes in predicted permeability. Equation (7) was empirically derived as part of this study. For the complete description of $\mu_c$ update routine, the reader is referred to [24] and the reference therein.

### C. DISPLACEMENT-DEPENDENT MAIN FLUX PATH AIR GAP RELUCTANCES

The main flux path reluctances are often the only type of air reluctances commonly considered for MC analysis. Because magnetic flux flows in a straight line in these reluctances, specifically main air gap $R_{g1}$ and side air gap $R_{g2}$ reluctances as shown in Fig. 4, they can be calculated using a simple relationship:

$$R_{gi} = \frac{x_i}{\mu_0 A_{gi}} = \frac{h_{gi} + x}{\mu_0 A_{gi}}, \tag{8}$$

where minimum air gaps in the closed state $h_{g1} = 0.2$ mm and $h_{g2} = 0.7$ mm, respectively.

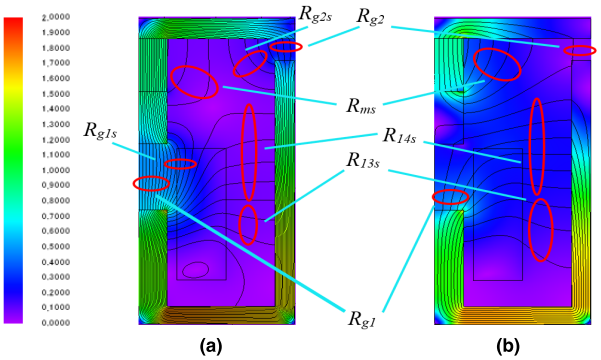


**FIGURE 4.** Magnetic field distribution and flux lines in the magnetic circuit of PM MC, and reluctances representing main, stray, and leakage flux paths in Fig. 2 (a). Colors represent the magnitude of flux density $B$ in T.

However, it is essential that (8) takes into account armature displacement because this allows the dynamics of PM MC to be reflected in ND-MEC. Considering armature motion is also an advantage of the stray flux path reluctance formulation discussed in the next section.

## III. STRAY PATH RELUCTANCES IN ND-MEC

### A. ELLIPTICAL MEAN PATH FUNCTION FOR STRAY AIR FLUX PATHS

This study defines all air magnetic flux paths other than the main and side air gap paths as stray flux paths, which in turn might be linked flux or leakage flux paths. The calculation of stray path reluctances is challenging because magnetic flux follows the paths of complex shapes. Conventionally, the same model, i.e., that with straight-line paths, was used for stray regions, while neglecting the distortion to the path and shape of the flux tube [25]. However, Sheikh-Ghalavand *et al.* and Yeo and Ro proposed the modeling of stray and leakage paths using circular arcs [26], [27]. Furthermore, Robertson *et al.* [28], [29] and Janssen *et al.* [30] and Tang *et al.* [31], as well as Ravaud *et al.* [32] and Babic and Akyel [33], proposed the use of an elliptical-like functions to model the interaction between the PM and coil, whereas Gabdullin and Ro recently proposed an algebraic representation for an elliptical flux path function that could be conveniently combined with MEC analysis for the purposes of stray flux calculation [24].

The latter function is modified in this study to reduce the computational cost of the path length calculation by considering the average length of the flux path. Fig. 5 illustrates an imaginary flux tube in the PM stray flux-region with a corresponding mean flux path, whose length must be calculated to represent this region in ND-MEC.

This study proposes to formulate the calculation in terms of parameters $f$ and $a_s$, as shown in Fig. 5. These parameters can be unambiguously determined considering the geometry of the stray flux region. For the example in Fig. 5, $f = h_m$, and the distance to the mean path in the tube $a_s = 0.25h_2$.

To find the ellipse arc length, the circumference of the ellipse is first calculated by rearranging Ramanujan's

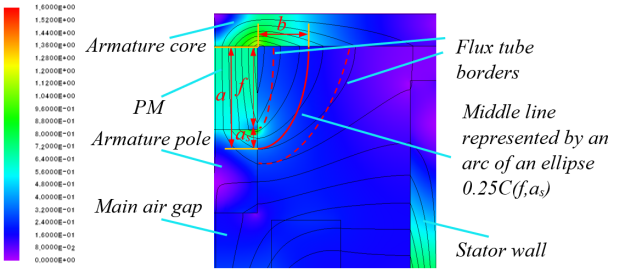


**FIGURE 5.** Methodology for the stray air path flux tube parameter evaluation for the PM $R_{ms}$ reluctance region including the mean elliptical arc length $C$, focal distance $f$, axes parameters $a$ and $b$, and mean step $a_s$. Colors represent the magnitude of flux density $B$ in T.

formula [34] as:

$$C(f, a_s) = \pi a(3 + 3k_a - \sqrt{3 + 4k_a + 3k_a^2}), \tag{9}$$

where

$$a = f + a_s \tag{10}$$

$$k_a = \left(\frac{a_s}{a}\right)^{1/2}. \tag{11}$$

It should be noted that the parameters $f$ and $a_s$ have the geometrical meanings of ellipse focal distance and semi-major axis, respectively. This formulation allows for the stray path reluctances to be evaluated as expression below:

$$R_s = \frac{l_{s.av}}{\mu_0 A_{s.av}} = \frac{k_e C(f, a_s)}{\mu_0 A_{s.av}}, \tag{12}$$

where $k_e$ is 0.5 or 0.25, depending on the type of elliptical arc that depends on the magnetic field distribution [24].

$A_{s.av}$ is an average cross-sectional area of the flux tube in a stray region that depends on the shape of the flux tube. Fig. 5 shows that flux tubes can have highly complex shapes, making $A_{s.av}$ calculation non-trivial. However, for this study, it is assumed that $A_{s.av}$ is the average of the areas of the magnetic core in regions where stray flux enters the flux guide.

It should be mentioned that the proposed modification to flux path calculation method is recommended when the field distribution does not possess significant non-homogeneities. The original method proposed in [24] was shown to generalize well and did not require prior knowledge about the shape of the flux tube. However, when the flux path shape is known and can be represented by a single elliptical arc, as in case of the studied PM MC, using the average flux path length significantly reduces the computational time without compromising the accuracy, as will be shown in Section VI.

### B. FORMULATION OF STRAY PATH RELUCTANCES USING THE PROPOSED ELLIPTICAL FUNCTION

#### 1) MAIN AND SIDE AIR GAP STRAY FLUX RELUCTANCES

Fig. 4 shows all stray regions that have to be represented in ND-MEC, with most conventional stray paths being those surrounding main and side gaps. First, by applying (12) to the main air gap region and considering a half-arc of an ellipse,

the main gap leakage reluctance is calculated as expressed below:

$$R_{g1s} = \frac{C(0.5x_1, 0.25h_2)}{\pi \mu_0 r_2 h_2}. \tag{13}$$

Second, by considering a quarter-arc inside the air gap region, one obtains:

$$R_{g2s} = \frac{C(x_2, 2x_2)}{16\mu_0 x_2 l_4}. \tag{14}$$

#### 2) THE PM AND COIL STRAY PATH RELUCTANCES

Fig. 3 shows that fluxes surrounding the PM can be leakage, as for attraction in Fig. 4 (a), and linked fluxes, as in Fig. 4 (b), because energy conversion occurs in the interior region of MC during repulsion. The PM stray flux reluctance is calculated considering a quarter-arc of an ellipse, as shown in Fig. 5, as:

$$R_{ms} = \frac{C(h_m, 0.25h_2)}{3\pi \mu_0 r_2 h_2}. \tag{15}$$

Finally, the paths that coil fluxes take during opening operation are represented by $R_{14s}$ reluctance, assuming that

$$a_{14s} = 0.5a_3 - r_1, \tag{16}$$

so that

$$R_{14s} = \frac{C(0.8a_{14s}, 0.2a_{14s})}{\pi \mu_0 r_1 x_1}. \tag{17}$$

This reluctance differs from others in that it has a constant path length and displacement-dependent cross-section; therefore, this path becomes more conductive with armature motion, unlike other air paths. This path potentially connects different parts of the stator instead of connecting the stator with the armature, making it contribute considerably to flux leakage during closing operation.

### C. CHARACYERIZATION OF COIL LEAKAGE PATHS USING THE PROPOSED CONCHOID ARC FUNCION

The paths for coil leakage fluxes are commonly represented by straight lines [35]. However, Fig. 4 shows that between stator poles and stator walls the field lines are distorted considerably, deviating from straight-line paths. To account for this distortion, this study proposes modeling coil leakage paths as arcs of a conchoid [36]. Considering the middle path in a flux tube in the same manner as for other stray paths, a conchoid representation allows accounting for the mentioned path distortion and calculating the path length [37] using:

$$L_c = \int \sqrt{r^2 + \left(\frac{dr}{d\theta}\right)^2}\, d\theta \tag{18}$$

where

$$r = c_1 + \frac{c_2}{cos\theta}, \tag{19}$$

and $c_1$, $c_2$ are parameters determining conchoid's shape. By substituting (19) into (18) and taking the derivative considering only $1.6\pi < \theta < 2.4\pi$ one obtains:

$$l_{13s} = L_c = \int_{1.6\pi}^{2.4\pi} \left( c_1 + \frac{2c_1c_2}{cos\theta} + \frac{c_2^2}{cos^2\theta} + \frac{c_2^2 sin^2\theta}{cos^4\theta} \right)^{0.5} d\theta. \tag{20}$$

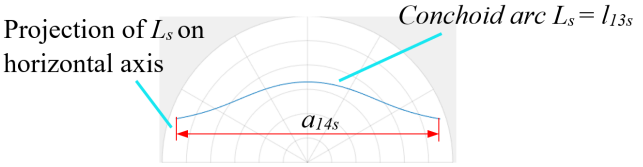


**FIGURE 6.** Determining the parameters of the conchoid arc $L_s$ to match the desired flux path length $l_{13s}$ by matching the projection of $L_s$ with the geometric parameters of PM MC $a_{14s}$.

Fig. 6 illustrates the shape of the conchoid arc that corresponds to (20). It should be noted that the parameters in (20) should be determined so that the desired shape is represented correctly. In limiting cases where $c_1 \gg c_2$ and $c_1 \ll c_2$, the shape of the conchoid arc in Fig. 6 approaches that of a semi-circle or a straight line, respectively.

Fig. 6 shows that $l_{13s}$ IS $L_c$ such that its projection on a horizontal axis is the distance between the stator pole and stator wall $a_{14s}$. Similar reasoning can be used to estimate flux paths in cases other than the studied PM MC. Table 1 summarizes the empirically determined parameters used to calculate $l_{13s}$ allowing stray path reluctance $R_{13s}$ to be calculated as:

$$R_{13s} = 4\frac{l_{13s}}{\mu_0 h_1 l_4}. \tag{21}$$

**TABLE 1.** Parameters for $l_{13s}$ calculation based on magnetic circuit geometry $a_{14s}$.

| Parameter | $c_1$ | $c_2$ | $\theta_1$ | $\theta_2$ | $l_{13s}$ |
|---|---|---|---|---|---|
| Value | 2.2 | 1.1 | $1.6\pi$ | $2.4\pi$ | 11.5 mm |

Similar to areas involved in previous reluctance calculations, areas contributing to this flux path should be carefully considered. In this case, the coil leakage flux connects a cylindrical stator pole with only two stators walls, but with the wall areas being much larger than that of the pole, resulting in a total multiplier of 4 in (21).

## IV. FLUX CALCULATION IN PM MC USING ND-MEC

### A. INVESTIGATING THE POSSIBILITY OF DESIGNING A ZERO-HOLDING-ENERGY PES

Fig. 2 (a) shows the complete ND-MEC including all reluctances previously discussed in this paper. However, this circuit can be reduced for flux calculation purposes by combining the reluctances [38], with the reduced version shown

in Fig. 2 (b). Specifically, the reluctances in the reduced ND-MEC Fig. 2 (b) are

$$R_{c13} = R_{c1} + R_{c2} + R_{c3} \tag{22}$$

$$R_{ma} = R_m + R_{c8} \tag{23}$$

$$R_{1eq} = R_{c10} + \left(\frac{1}{R_{g1}} + \frac{1}{R_{g1s}}\right)^{-1} \tag{24}$$

$$R_{2eq} = R_{c5} + R_{c7} + \left(\frac{1}{R_{g2s}} + \frac{1}{R_{g2} + R_{c6}}\right)^{-1} \tag{25}$$

The ND-MEC equations are solved using the matrix form of the mesh current method, numbering loop fluxes as shown in Fig. 2 (b). This allows the use of the matrix form so that:

$$\begin{bmatrix} F_C \\ 0 \\ 0 \\ F_m \end{bmatrix} = R_t \cdot \begin{bmatrix} \Phi_1 \\ \Phi_2 \\ \Phi_3 \\ \Phi_4 \end{bmatrix}, \tag{26}$$

where

$$R_t = \begin{bmatrix} R_{11} & -R_{13s} & 0 & 0 \\ -R_{13s} & R_{22} & -R_{14s} & 0 \\ 0 & -R_{14s} & R_{33} & -R_{ms} \\ 0 & 0 & -R_{ms} & R_{44} \end{bmatrix} \tag{27}$$

and

$$R_{11} = R_{c13} + R_{13s} \tag{28}$$

$$R_{22} = R_{1\mathrm{eq}} + R_{13s} + R_{14s} + R_{c4} \tag{29}$$

$$R_{33} = R_{14s} + R_{2eq} + R_{c9} + R_{ms} \tag{30}$$

$$R_{44} = R_{\mathrm{ms}} + R_{ma} \tag{31}$$

Equation (26) is solved for loop fluxes, so that fluxes in every branch of ND-MEC in Fig. 2 (a) can be calculated using the known rules of electric circuit theory [38].

## V. PM MC FORCE CALCULATION USING NT-PEM

### A. ELECTROMAGNETIC FORCE CALCULATION

This study employs the NT-PEM to evaluate the complete dynamics of the PM MC. For the complete description of the method, the reader is referred to [24], with the temporal discretization method described in [39], [40]. For this study, it should be mentioned that NT-PEM relies on solving the ND-MEC discussed in Sections II–IV for different positions of the armature $x$ and varying coil current $I_c$ to represent the closing and opening operations of the PM MC over $n$ steps. The data obtained from two consecutive solutions is then used to calculate electromagnetic force using the path energy method as:

$$F^n_{mag}(I_c, x) = -\frac{{W_{mag}}^n(I_c, x) - {W_{mag}}^{n-1}(I_c, x)}{dx^n} \tag{32}$$

and

$$W^n_{mag}(I_c, x) = \sum_i (k^n_{wi})^2 \frac{(B^n_i)^2}{2\mu_0} \cdot V^n_i, \tag{33}$$

where the summation is performed for all air regions, and $k_w$ adjusts the air region magnetic energy contributions to the force. It can also be treated as a parameter storing the information about the local orientation of the electromagnetic force vector. Conventionally, MEC methods do not allow for spatial components of field vectors to be estimated. However, formulation (33) used to quantify air flux paths provides an opportunity to estimate the shape of the path. For vertical flux paths in Fig. 4:

$$k_{wi} = \frac{4a_i}{\mathrm{C}_i(f_i, a_{si})}, \tag{34}$$

and for horizontal flux paths:

$$k_{wi} = \frac{4b_i}{\mathrm{C}_i(f_i, a_{si})}. \tag{35}$$

Equation (34) applies to all regions but the $R_{14s}$ region. To calculate $k_{w14s}$, the semi-minor axis of the ellipse $b_{14s}$ should be calculated taking (16) into account:

$$b_{14s} = a_{14s}\sqrt{1 - \frac{f_{14s}}{a_{14s}}} \approx 0.45a_{14s} \tag{36}$$

and

$$k_{w14s} = \frac{1.8a_{14s}}{C_{14s}}. \tag{37}$$

**TABLE 2. Closing (Cl) and opening (Op) path energy coefficients $k_w$.**

| Reg. | $k_{wg1}$ | $k_{wg1s}$ | $k_{wg2}$ | $k_{wg2s}$ | $k_{wms}$ | $k_{w13s}$ | $k_{w14s}$ |
|---|---|---|---|---|---|---|---|
| *Cl.* | 1 | $\frac{2x_1 + h_2}{C_{g1s}}$ | 1 | $\frac{12x_2}{C_{g2s}}$ | 0 | 0 | $\frac{1.8a_{14s}}{C_{14s}}$ |
| *Op.* | | | | | $\frac{4h_m + h_2}{C_{ms}}$ | | |

Table 2 summarizes $k_w$ calculated using (34) and the parameters in (13)–(17). The geometrical meaning of $k_w$ is a ratio of the semi-major (34) or semi-minor (35) axes to the flux path length. Because ellipse axes are always oriented either vertically or horizontally in the proposed method, (34) and (35) ensure that the information about spatial components of the magnetic flux vectors is stored in $k_w$ to be used for force calculation.

It should be noted that the roles of some reluctances change depending on the regime. For instance, reluctances $R_{g1s}$ and $R_{g2s}$ are crucial for closing operation, whereas $R_{ms}$ and $R_{14s}$ are leakage reluctances in this regime. On the contrary, $R_{ms}$ and $R_{14s}$ participate in energy conversion during opening due to the change in magnetic field distribution (see Fig. 4 (b)), but $R_{g1s}$ and $R_{g2s}$ conduct nearly no flux. For both regimes, $R_{13s}$ is a leakage reluctance not participating in energy conversion, as reflected in its $k_{w13s}$ in Table 2.

### B. PROPOSED FORMULATION OF ELECTRICAL CIRCUIT EQUATIONS

To model the complete transient behavior of PM MC, the equations for an electrical circuit in Fig. 7 are formulated so to account for electromagnetic and mechanical effects, and

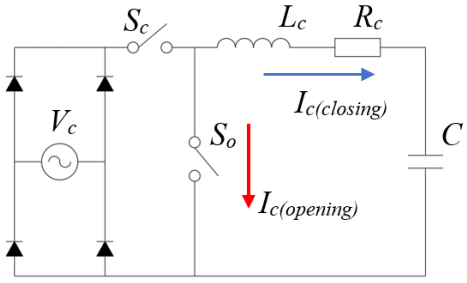


**FIGURE 7.** Proposed electric circuit for the single-coil PM MC. By closing switch $S_c$, the MC coil and capacitor $C$ are connected to the voltage source $V_c$, which initiates closing by inducing closing current and charging the capacitor. For the opening operation to start, the switch $S_o$ is closed, allowing the capacitor to discharge by inducing opening current in the PM MC coil.

extended to time domain resulting in the following system of equations for an $n^{th}$ step [41], [42]:

$$\begin{cases} V_s^n = \left(I_c^{n-1} + dI_c^n\right) R_c + L_{ci}^{n-1} \dfrac{dI_c^n}{dt} + L_{cx}^{n-1} \dfrac{dx^n}{dt} \\ L_{ci}^n = \dfrac{\lambda_c^n (I_c, x) - \lambda_c^{n-1} (I_c, x)}{di^n} \\ L_{cx}^n = \dfrac{\lambda_c^n (I_c, x) - \lambda_c^{n-1} (I_c, x)}{dx^n} \\ dI_c{}^n = \dfrac{\left(V_s^n - I_c^{n-1} R_c\right) dt - L_{cx}^{n-1} dx^n}{R_c dt + L_{ci}^{n-1}}, \end{cases} \tag{38}$$

where $V_s$ is the applied voltage in V, $dI_c$ is the current increment in A, $R_c$ is the coil resistance in ohm, $L_{ci}$ is the coil inductance characterizing the transformer electromotive force (emf) in H, $L_{cx}$ is the inductance characterizing motional emf in Wb/m, $\lambda_c$ is the linked flux in Wb, $t$ is time in s, and $dt$ is the time increment in s.

### C. PROPOSED FORMULATION OF ELECTRICAL CIRCUIT EQUATIONS

Motion equations for an $n^{th}$ step are expressed using Newton's equations of motion as:

$$\begin{cases} F_{net}^n(i, x) = F_g + F_{mag}^n(i, x) + F_{spring}^n(x) \\ v^n = v^{n-1} + \left(\dfrac{F_{net}^n(i, x)}{m}\right) dt \\ x^n = x^{n-1} + [v^{n-1} dt + \dfrac{1}{2} \left(\dfrac{F_{net}^n(i, x)}{m}\right) (dt)^2], \end{cases} \tag{39}$$

where $F_g$ is the gravitational force in N, $F_{spring}$ is the opening spring force in N, $v$ is the velocity in m/s, and $m$ is the armature mass with moving contacts in kg. The opening spring is designed following the recently proposed methodology considering the desired holding force of the PM [7].

## VI. RESULTS AND DISCUSSION

### A. ANALYSIS RESULTS OF THE CLOSING OPERATION OF THE PM MC

The closing operation is initiated by closing the switch $S_c$ connecting the voltage source $V_c$ to the coil, as shown in Fig. 7. Figs. 8 and 9 show that the closing operation concludes in 8 ms with the electromagnetic force in Fig. 8 following the waveform of coil current until the PM MC armature reaches the closed state position and electromagnetic force reaches holding force value.

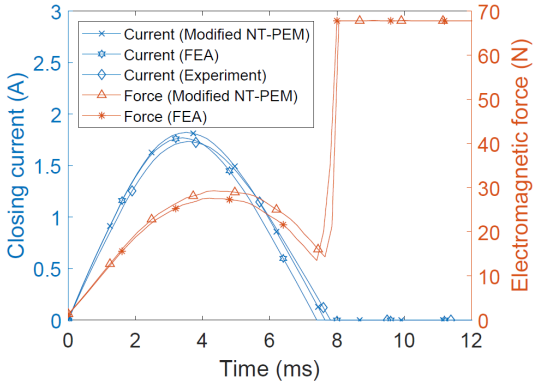


**FIGURE 8.** Comparison of simulation (NT-PEM, 3D FEA) results and experimental data for the coil current and electromagnetic force of a single-coil PM MC during the closing operation.

Because the holding force provided by the PM is sufficient to maintain the closed state of the PM MC, the input voltage is removed by opening $S_c$ after the coil current reaches zero in Fig. 8. This prevents unnecessary energy loss during holding, which occurs in case of solenoid MC. The ability of PM MC to maintain a closed state with no power consumption is a significant advantage that makes it more cost-efficient and eco-friendlier than the conventional solenoid MCs [11].

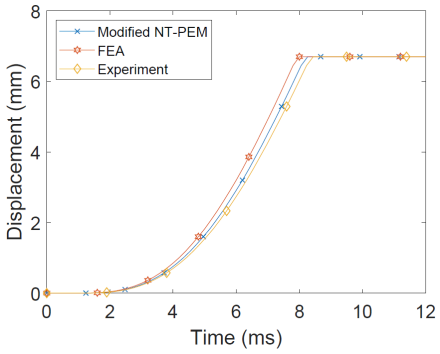


**FIGURE 9.** Comparison of simulation results and experimental data for the armature displacement of a single-coil PM MC during the closing operation.

### B. ANALYSIS RESULTS OF THE OPENING OPERATION OF PM MC

To open the PM MC, switch $S_o$ is closed, allowing the capacitor C to discharge, thereby inducing a reverse current in the coil, which results in a repulsive electromagnetic force between the coil and PM. At the beginning of the opening operation, the holding force decreases as the opening current increases as shown in Fig. 10, with no initial motion of the armature in Fig. 11. As current becomes sufficient at around 1 ms, the repulsive electromagnetic force starts increasing and propagates the armature to the open state position.

As in case of closing, no continues current is required to maintain the open state after capacitor discharges. Due to the large air gap that also ensures reliable braking of the current

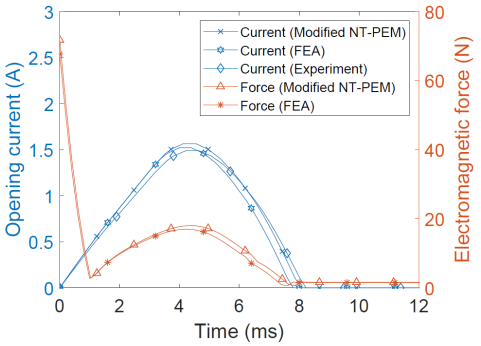


**FIGURE 10.** Comparison of simulation results and experimental data for the coil current and electromagnetic force of a single-coil PM MC during opening operation.

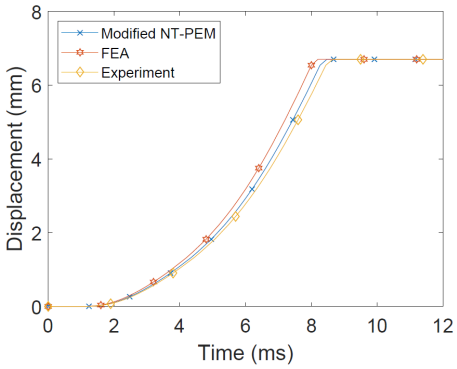


**FIGURE 11.** Comparison of simulation results and experimental data for the armature displacement of a single-coil PM MC during the opening operation.

controlled by the MC [43], the electromagnetic force of the PM in an open state is not sufficient to close the PM MC. Thus, it remains open until the closing voltage is applied, and the described operating sequence is repeated.

It should be noted that the force was not measured during the experiment due to the extremely large displacement of PM MC armature that complicates the measurement using conventional force probes. The large displacement is a design requirement due to the necessity to reliably separate stationary and moving contacts. However, measuring the displacement is sufficient to verify the feasibility of the designed PM MC. Fig. 11 shows that PM MC armature successfully reaches its open state position in under 10 ms indicating high-speed breaking that is the most important parameter for evaluating the PM MC dynamics. This approach is commonly used to verify the feasibility of PM MCs without measuring the force as in [6], [8]–[11], [19], [42], and [43].

### C. ACCURACY AND SPEED OF THE PROPOSED ANALYSIS METHOD

Figs. 8–11 show that NT-PEM and FEA conducted using JMAG provide comparable accuracies with errors not exceeding 5% when compared to the experimental data. However, the analysis time is significantly reduced by implementing the proposed analytical method, as shown in Table 3. The short analysis time of the previously proposed NT-PEM was further reduced in this study by considering the average flux path lengths for stray air paths and the more computationally stable permeability update routine (7), as discussed in Sections II and III. Specifically, the proposed modifications resulted in a four times faster analysis, leading to a total of a 2000-fold difference in the analysis times between the modified NT-PEM and FEA. This reduction in computational costs has the most significant impact when numerous designs are to be considered, as in the case of preliminary design and the final design optimization [44].

**TABLE 3.** Computational time of the FEA, Original NT-PEM and the modified NT-PEM of comparable accuracy with <5% error.

| Method | Analysis time | Time reduction ratio |
|---|---|---|
| FEA (JMAG) | 1 h | 1 |
| NT-PEM [24] | 7.2 s | 500 |
| Modified NT-PEM (this study) | 1.8 s | 2000 |

It is noteworthy that the computational time in FEA depends on the sizes of the mesh element as well as the model size, leading to an enormous number of equations to be solved for large 3D models [45]. However, the computational time of NT-PEM depends on the complexity of the ND-MEC, i.e., the number of branches and matrix size in (27) and not on the physical size of the analyzed model. This implies that by carefully choosing an ND-MEC and reducing its complexity according to the recommendations presented in this study, the computational costs of NT-PEM can be expected to increase with the size of the analyzed contactor slower than in the case of FEA. Thus, the computational time ratio in Table 3 calculated for a small contactor can be expected to be even more significant for larger contactors, thereby implying better scalability of the NT-PEM than that of the FEA when computational cost and speed are considered.

## VII. CONCLUSION

This study proposes a modification to the recently proposed accurate and computationally inexpensive NT-PEM. It uses a single ND-MEC to represent both the closing and opening regimes of a single-coil PM MC with lengths of stray flux paths evaluated using the proposed elliptical and conchoid functions. The proposed ND-MEC topology, along with an accurate calculation of flux path lengths, allows for stray and leakage flux paths to be represented correctly, unlike in conventional MECs with simplified path shapes. The overall analysis speed is enhanced by considering only average flux path lengths while avoiding iterative flux path calculation routines of the original NT-PEM. Furthermore, a computationally robust correction to the permeability update routine in ND-MEC is proposed, with all modifications combined resulting in an analysis time of the modified NT-PEM that is four times shorter than that of the original version of the proposed method.

The comparison of the modified NT-PEM with FEA shows up to a 2000-fold enhancement in computational speed for comparable accuracies with errors not exceeding 5%. The feasibility of the proposed method is verified using experimental data obtained from a single-coil PM MC prototype. This result indicates significant potential for the modified NT-PEM to be applied as an accurate and computationally efficient alternative to the FEA for solving various design and optimization problems when numerous designs must be considered.

Future work will include the flux distribution study in stray and leakage regions of PM MC with flux measurement conducted using Hall probe for further verification of the proposed elliptical and conchoids functions. Higher power level single coil PM MCs will also be studied to verify opening speed and opening-closing commutation feasibility to simplify the design of conventional double-coil PM MCs.

## REFERENCES


[1] D. T. Danielson, "Barriers to industrial energy efficiency," U.S. Dept. Energy, Washington, DC, USA, Tech. Rep., Jun. 2015. [Online]. Available: https://www.energy.gov/eere/amo/downloads/barriers-industrial-energy-efficiency-report-congress-june-2015

[2] United States Environmental Protection Agency (EPA). *Greenhouse Gas Emissions*. Accessed: Jun. 4, 2019. [Online]. Available: https://www.epa.gov/ghgemissions

[3] F. A. Chachar, S. S. H. Bukhari, F. H. Mangi, D. E. Macpherson, G. P. Harrison, W. Bukhsh, and J.-S. Ro, "Hierarchical control implementation for meshed AC/multi-terminal DC grids with offshore windfarms integration," *IEEE Access*, vol. 7, pp. 142233–142245, 2019, doi: 10.1109/access.2019.2944718.

[4] X. Liu, X. Wang, and J. Wen, "Optimal power flow of DC-grid based on improved PSO algorithm," *J. Electr. Eng. Technol.*, vol. 12, no. 4, pp. 1586–1591, 2017, doi: 10.5370/JEET.2017.12.4.1586.

[5] S. Y. Lin and X. S. Huang, "Power loss analysis of AC contactor at steady closed state with electromagnetic-thermal coupling method," *J. Inf. Hiding Multimedia Signal Process.*, vol. 8, no. 2, pp. 290–299, 2017.

[6] S. Fang, Q. Liu, H. Lin, and S. L. Ho, "A novel flux-weakening control strategy for permanent-magnet actuator of vacuum circuit breaker," *IEEE Trans. Ind. Electron.*, vol. 63, no. 4, pp. 2275–2283, Apr. 2016, doi: 10.1109/TIE.2015.2500182.

[7] L. Shu, L. Wu, G. Wu, and Z. Wu, "A fully coupled framework of predicting the dynamic characteristics of permanent magnet contactor," *IEEE Trans. Magn.*, vol. 52, no. 8, Aug. 2016, Art. no. 8001607, doi: 10.1109/TMAG.2016.2557310.

[8] Z. Wang, L. Sun, S. He, Y. Geng, and Z. Liu, "A permanent magnetic actuator for 126 kV vacuum circuit breakers," *IEEE Trans. Magn.*, vol. 50, no. 3, pp. 129–135, Mar. 2014, doi: 10.1109/TMAG.2013.2284251.

[9] H.-J. Park, S.-H. Kim, J.-S. Ro, and H.-K. Jung, "Analysis and design of separated permanent magnet actuator for 225AF molded case circuit breaker," in *Proc. 17th Int. Conf. Electr. Mach. Syst. (ICEMS)*, Oct. 2014, pp. 2888–2891, doi: 10.1109/ICEMS.2014.7013990.

[10] H.-J. Bak, J.-S. Ro, T.-K. Chung, and H.-K. Jung, "Characteristics analysis and design of a novel magnetic contactor for a 220 V/85 a," *IEEE Trans. Magn.*, vol. 49, no. 11, pp. 5498–5506, Nov. 2013, doi: 10.1109/TMAG.2013.2268054.

[11] N. Gabdullin and J.-S. Ro, "Energy-efficient eco-friendly zero-holding-energy magnetic contactor for industrial and vehicular applications," *IEEE Trans. Veh. Technol.*, early access, doi: 10.1109/TVT.2020.2981888.

[12] M. M. Zaid and J.-S. Ro, "Switch ladder modified H-Bridge multilevel inverter with novel pulse width modulation technique," *IEEE Access*, vol. 7, pp. 102073–102086, 2019, doi: 10.1109/access.2019.2930720.

[13] S. Madanzadeh, A. Abedini, A. Radan, and J.-S. Ro, "Application of quadratic linearization state feedback control with hysteresis reference reformer to improve the dynamic response of interior permanent magnet synchronous motors," *ISA Trans.*, early access, Sep. 5, 2019, doi: 10.1016/j.isatra.2019.08.067.

[14] S. Khan, S. S. H. Bukhari, and J.-S. Ro, "Design and analysis of a 4-kW two-stack coreless axial flux permanent magnet synchronous machine for low-speed applications," *IEEE Access*, vol. 7, pp. 173848–173854, 2019, doi: 10.1109/ACCESS.2019.2957046.

[15] J. Duan, S. Xiao, K. Zhang, and Y. Jing, "A novel 3-D analytical modeling method of trapezoidal shape permanent magnet Halbach array for multi-objective optimization," *J. Electr. Eng. Technol.*, vol. 14, no. 2, pp. 635–643, Mar. 2019, doi: 10.1007/s42835-019-00109-w.

[16] C. Luo, K. Zhang, J. Duan, and Y. Jing, "Study of permanent magnet electrodynamic suspension system with a novel Halbach array," *J. Electr. Eng. Technol.*, vol. 15, no. 2, pp. 969–977, Mar. 2020, doi: 10.1007/s42835-019-00342-3.

[17] M.-F. Hsieh and Y.-C. Hsu, "A generalized magnetic circuit modeling approach for design of surface permanent-magnet machines," *IEEE Trans. Ind. Electron.*, vol. 59, no. 2, pp. 779–792, Feb. 2012, doi: 10.1109/TIE.2011.2161251.

[18] B. Chen, "Analysis of effect of winding interleaving on leakage inductance and winding loss of high frequency transformers," *J. Electr. Eng. Technol.*, vol. 14, no. 3, pp. 1211–1221, May 2019, doi: 10.1007/s42835-019-00129-6.

[19] E. Ramirez-Laboreo, C. Sagues, and S. Llorente, "A new model of electromechanical relays for predicting the motion and electromagnetic dynamics," *IEEE Trans. Ind. Appl.*, vol. 52, no. 3, pp. 2545–2553, May 2016, doi: 10.1109/TIA.2016.2518120.

[20] D. Faustner, W. Kemmetmüller, and A. Kugi, "Magnetic equivalent circuit modeling of a saturated surface-mounted permanent magnet synchronous machine," *IFAC-PapersOnLine*, vol. 48, no. 1, pp. 360–365, 2015, doi: 10.1016/j.ifacol.2015.05.033.

[21] J. Bao, B. L. J. Gysen, and E. A. Lomonova, "Hybrid analytical modeling of saturated linear and rotary electrical machines: Integration of Fourier modeling and magnetic equivalent circuits," *IEEE Trans. Magn.*, vol. 54, no. 11, Nov. 2018, Art. no. 8109905, doi: 10.1109/TMAG.2018.2837896.

[22] S. A. Randi, R. Benlamine, F. Dubas, and C. Espanet, "Semi-analytical method based on magnetic equivalent circuit in EV and HEV applications," *Mediterr. J. Model. Simul.*, vol. 1, no. 1, pp. 1–12, 2014.

[23] P. Diez and J. P. Webb, "A rational approach to $B - H$ curve representation," *IEEE Trans. Magn.*, vol. 52, no. 3, Mar. 2016, Art. no. 7203604, doi: 10.1109/TMAG.2015.2488360.

[24] N. Gabdullin and J.-S. Ro, "Novel non-linear transient path energy method for the analytical analysis of the non-periodic and non-linear dynamics of electrical machines in the time domain," *IEEE Access*, vol. 7, pp. 37833–37854, 2019, doi: 10.1109/ACCESS.2019.2905856.

[25] A. Stuikys, M. Rotaru, and J. K. Sykulski, "A refined approach exploiting tubes of flux for analysis of linear switched reluctance motors," *Int. J. Appl. Electromagn. Mech.*, vol. 51, no. s1, pp. S13–S21, Apr. 2016, doi: 10.3233/JAE-2022.

[26] B. Sheikh-Ghalavand, S. Vaez-Zadeh, and A. H. Isfahani, "An improved magnetic equivalent circuit model for iron-core linear permanent-magnet synchronous motors," *IEEE Trans. Magn.*, vol. 46, no. 1, pp. 112–120, Jan. 2010, doi: 10.1109/TMAG.2009.2030674.

[27] H.-K. Yeo and J.-S. Ro, "Novel analytical method for overhang effects in surface-mounted permanent-magnet machines," *IEEE Access*, vol. 7, pp. 148453–148461, 2019, doi: 10.1109/access.2019.2939939.

[28] W. Robertson, B. Cazzolato, and A. Zander, "A simplified force equation for coaxial cylindrical magnets and thin coils," *IEEE Trans. Magn.*, vol. 47, no. 8, pp. 2045–2049, Aug. 2011, doi: 10.1109/TMAG.2011.2129524.

[29] W. Robertson, B. Cazzolato, and A. Zander, "Axial force between a thick coil and a cylindrical permanent magnet: Optimizing the geometry of an electromagnetic actuator," *IEEE Trans. Magn.*, vol. 48, no. 9, pp. 2479–2487, Sep. 2012, doi: 10.1109/TMAG.2012.2194789.

[30] J. L. G. Janssen, J. J. H. Paulides, E. A. Lomonova, and A. J. A. Vandenput, "Analysis of a variable reluctance permanent magnet actuator," in *Proc. IEEE Ind. Appl. Annu. Meeting*, Sep. 2007, pp. 502–509, doi: 10.1109/07IAS.2007.45.

[31] Y. Tang, J. J. H. Paulides, and E. A. Lomonova, "Analytical modeling of flux-switching in-wheel motor using variable magnetic equivalent circuits," *ISRN Automot. Eng.*, vol. 2014, pp. 1–10, Jan. 2014, doi: 10.1155/2014/530260.

[32] R. Ravaud, G. Lemarquand, S. Babic, V. Lemarquand, and C. Akyel, "Cylindrical magnets and coils: Fields, forces, and inductances," *IEEE Trans. Magn.*, vol. 46, no. 9, pp. 3585–3590, Sep. 2010, doi: 10.1109/TMAG.2010.2049026.

[33] S. I. Babic and C. Akyel, "Magnetic force calculation between thin coaxial circular coils in air," *IEEE Trans. Magn.*, vol. 44, no. 4, pp. 445–452, Apr. 2008, doi: 10.1109/TMAG.2007.915292.
[34] M. B. Villarino, "Ramanujan's perimeter of an ellipse," 2005, *arXiv:math/0506384*. Accessed: Dec. 4, 2019. [Online]. Available: https://arxiv.org/abs/math/0506384
[35] J.-M. Seo, I.-S. Jung, H.-K. Jung, and J.-S. Ro, "Analysis of overhang effect for a surface-mounted permanent magnet machine using a lumped magnetic circuit model," *IEEE Trans. Magn.*, vol. 50, no. 5, May 2014, Art. no. 8201207, doi: 10.1109/TMAG.2013.2294154.
[36] F. Szmulowicz, "Conchoid of Nicomedes from reflections and refractions in a cone," *Amer. J. Phys.*, vol. 64, no. 4, pp. 467–471, Apr. 1996.
[37] *Conchoid of Nicomedes*. Accessed: Oct. 2, 2019. [Online]. Available: http://users.math.uoc.gr/ pamfilos/eGallery/problems/Nicomedes.html
[38] A. H. Robbins and W. C. Miller, *Circuit Analysis: Theory and Practice*, 3rd ed. Boston, MA, USA: Delmar, 2003.
[39] K. A. Hoffmann and S. T. Chiang, *Computational Fluid Dynamics for Engineers*, 4th ed. Wichita, KS, USA: Engineering Education System, 1993.
[40] D.-J. Cho, D.-K. Woo, J.-S. Ro, T.-K. Chung, and H.-K. Jung, "Novel electromagnetic actuator using a permanent magnet and an inter-locking mechanism for a magnetic switch," *IEEE Trans. Magn.*, vol. 49, no. 5, pp. 2229–2232, May 2013, doi: 10.1109/TMAG.2013.2242432.
[41] J.-S. Rho, C.-H. Lee, and H.-K. Jung, "Characteristic analysis and design of a small size rotary ultrasonic motor using the cutting method," *Int. J. Appl. Electromagn. Mech.*, vol. 28, no. 4, pp. 469–500, Dec. 2008.
[42] H.-J. Park, J.-S. Ro, K.-P. Yi, T.-K. Chung, and H.-K. Jung, "Dynamic analysis and design of an armature for an inter-locking system of a magnetic contactor," in *Proc. Int. Conf. Electr. Mach. Syst. (ICEMS)*, Oct. 2013, pp. 676–679.
[43] Y. Han, W. Shang, C. Hou, A. Li, and Y. Cao, "Study on factors influencing the characteristics of arc in DC contactors," in *Proc. 4th Int. Conf. Electr. Power Equip.-Switching Technol. (ICEPE-ST)*, Oct. 2017, pp. 406–410, doi: 10.1109/ICEPE-ST.2017.8188886.
[44] A. Stuikys and J. Sykulski, "Rapid multi-objective design optimisation of switched reluctance motors exploiting magnetic flux tubes," *IET Sci., Meas. Technol.*, vol. 12, no. 2, pp. 223–229, Mar. 2018, doi: 10.1049/iet-smt.2017.0213.
[45] O. C. Zienkiewicz, R. L. Taylor, and J. Z. Zhu, *The Finite Element Method: Its Basis and Fundamentals*, 6th ed. Amsterdam, The Netherlands: Elsevier, 2005.

**NIKITA GABDULLIN** (Member, IEEE) received the B.S. and M.S. degrees in electrical engineering from National Research University "MPEI," Moscow, Russia, in 2010 and 2012, respectively, and the Ph.D. degree in electrical and electronic engineering from City, University of London, London, U.K., in 2017.

He is currently a Postdoctoral Researcher with Chung-Ang University, Seoul, South Korea. His research interests include analytical and numerical modeling of electromagnetic fields, novel electrical machine design, multiphysics and coupled problem analysis, smart materials, and application of energy-efficient electromagnetic smart devices.

**JONG-SUK RO** (Member, IEEE) received the B.S. degree in mechanical engineering from Hanyang University, Seoul, South Korea, in 2001, and the Ph.D. degree in electrical engineering from Seoul National University (SNU), Seoul, in 2008.

He conducted research at the Research and Development Center, Samsung Electronics, as a Senior Engineer, from 2008 to 2012. From 2012 to 2013, he was with the Brain Korea 21 Information Technology, SNU, as a Postdoctoral Fellow. From 2013 to 2016, he worked with the Brain Korea 21 Plus, SNU, as an Assistant Professor. He conducted research at the Electrical Energy Conversion System Research Division, Korea Electrical Engineering and Science Research Institute, as a Researcher, in 2013. In 2014, he was an Academic Visitor with the University of Bath, Bath, U.K. He is currently an Associate Professor with the School of Electrical and Electronics Engineering, Chung-Ang University, Seoul. His research interests include the analysis and optimal design of next-generation electrical machines using smart materials, such as electromagnet, piezoelectric, and magnetic shape memory alloy.